Received: 19 February 2025 | Revised: 11 July 2025 | Accepted: 14 July 2025

DOI: 10.1002/alz.70570

Alzheimer's & Dementia®
THE JOURNAL OF THE ALZHEIMER'S ASSOCIATION

RESEARCH ARTICLE

Free water predicts dementia with Lewy bodies in isolated REM sleep behavior disorder

Celine Haddad[1,2] | Véronique Daneault[1] | Violette Ayral[1,3] | Marie Filiatrault[1,3] | Alexandre Pastor-Bernier[1] | Christina Tremblay[1] | Arnaud Boré[4] | Maxime Descoteaux[4] | Andrew Vo[5] | Jean-François Gagnon[1,6,7] | Ronald B. Postuma[1,8] | Petr Dusek[9] | Stanislav Marecek[9] | Zsoka Varga[9] | Johannes Klein[10] | Michele T. Hu[10] | Stéphane Lehéricy[11] | Isabelle Arnulf[11] | Marie Vidailhet[11] | Jean-Christophe Corvol[11] | ICEBERG Study Group[11] | Shady Rahayel[1,12]

[1]Centre for Advanced Research in Sleep Medicine, Hôpital du Sacré-Cœur de Montréal, CIUSSS-NÎM, Montreal, Canada

[2]Department of Psychology, University of Montreal, Montreal, Canada

[3]Department of Neuroscience, University of Montreal, Montreal, Canada

[4]Sherbrooke Connectivity Imaging Lab, University of Sherbrooke, Sherbrooke, Canada

[5]The Neuro (Montreal Neurological Institute-Hospital), McGill University, Montreal, Canada

[6]Department of Psychology, Université du Québec à Montréal, Montreal, Canada

[7]Research Centre, Institut universitaire de gériatrie de Montréal, Montreal, Canada

[8]Department of Neurology, Montreal General Hospital, Montreal, Canada

[9]Department of Neurology and Centre of Clinical Neurosciences, First Faculty of Medicine, Charles University and General University Hospital, Prague, Czechia

[10]Oxford Parkinson's Disease Centre and Division of Neurology, Nuffield Department of Clinical Neurosciences, University of Oxford, Oxford, UK

[11]Institut du Cerveau, Paris Brain Institute, ICM, Assistance Publique Hôpitaux de Paris, Sorbonne Université, Paris, France

[12]Department of Medicine, University of Montreal, Montreal, Canada

Correspondence
Shady Rahayel, Center for Advanced Research in Sleep Medicine, 5400 West Gouin Boulevard, Montreal, Quebec, Canada.
Email: shady.rahayel@umontreal.ca

Abstract

INTRODUCTION: Most individuals with isolated rapid eye movement sleep behavior disorder (iRBD) develop dementia with Lewy bodies (DLB) or Parkinson's disease (PD). Brain biomarkers predicting specific phenoconversion trajectories are lacking.

Funding information: Canadian Institutes of Health Research; Roche; Parkinson's Foundation; Michael J. Fox Foundation; R. Howard Webster Foundation; International Parkinson and Movement Disorders Society; Parkinson Canada, Grant/Award Number: PPG-2023-0000000122; Alzheimer Society Canada, Grant/Award Number: 0000000082; Programme d'investissements d'avenir, Grant/Award Number: ANR-10-IAIHU-06; Paris Institute of Neurosciences–IHU, Grant/Award Number: IAIHU-06; Agence Nationale de la Recherche, Grant/Award Number: ANR-11-INBS-0006; Électricité de France; Fondation d'Entreprise EDF; Biogen Inc.; Fonds Saint-Michel; Société Française de Médecine Esthétique; Institut de France; Fonds de recherche du Québec–Santé; W. Garfield Weston Foundation; NIH/National Institute on Aging; Parkinson's UK, Grant/Award Number: J-2101; Oxford Biomedical Research Centre (BRC); Czech Health Research Council, Grant/Award Numbers: NU21-04-00535, LX22NPO5107; 4D Pharma; AbbVie Inc.; AcureX Therapeutics; Allergan; Aligning Science Across Parkinson's (ASAP); Avid Radiopharmaceuticals; Bial Biotech; BioLegend; Bristol Myers Squibb; Calico Life Sciences LLC; Celgene Corporation; DaCapo Brainscience; Denali Therapeutics; Edmond J. Safra Foundation; Eli Lilly and Company; GE Healthcare; GlaxoSmithKline; Golub Capital; Handl Therapeutics; Insitro; LLC; Piramal Imaging; Prevail Therapeutics; F. Hoffman-La Roche Ltd.; Genentech Inc.; Teva Neuroscience, Inc.; Vanqua Bio; Voyager Therapeutics, Inc.; Yumanity Therapeutics, Inc.

List of contributors involved in the ICEBERG Study Group is available in the Appendix section.

METHODS: In this multicenter diffusion magnetic resonance imaging study (261 iRBD, 177 controls), free water (FW) was measured in the nucleus basalis of Meynert (NBM) and posterior substantia nigra (SN). Among 230 iRBD patients with follow-up, 64 converted (16 DLB, 38 PD). Time-to-event analyses were performed to assess differential phenoconversion.

RESULTS: Phenoconverters had higher FW in the NBM and posterior SN. Only FW in the NBM predicted conversion to DLB over PD. NBM volume predicted DLB conversion, but only FW remained significant when both were modeled. FW in the NBM correlated with lower MoCA scores in iRBD.

DISCUSSION: FW in the NBM is a sensitive biomarker of cognitive decline and DLB progression in iRBD, outperforming volume and supporting its use in early stratification.

KEYWORDS
biomarker, dementia with Lewy bodies, diffusion magnetic resonance imaging, free water, Parkinson's disease, prognosis, REM sleep behavior disorder

Highlights

- FW in the NBM specifically identifies conversion to DLB.
- Increased FW in the NBM is associated with lower global cognition in iRBD.
- FW in the SN in iRBD does not relate more to DLB than PD.
- FW in the NBM is a biomarker of differential phenoconversion in iRBD.

1 | BACKGROUND

Isolated rapid eye movement (REM) sleep behavior disorder (iRBD) is a parasomnia characterized by the loss of normal muscle atonia during REM sleep, resulting in abnormal and often violent movements and vocalizations.[1] It is widely recognized as an early manifestation of synucleinopathies such as dementia with Lewy bodies (DLB), Parkinson's disease (PD), and multiple system atrophy (MSA) with over 90% of individuals progressing to one of these diseases within 15 years.[2] Patients with iRBD experience brain changes similar to those seen in overt synucleinopathies, including brain atrophy,[3–9] abnormal perfusion,[10–14] and reduced striatal dopamine transporter binding.[15–17] Although existing imaging markers have been examined as potential predictors of disease progression, they have rarely been tested in large multicentric studies or across varying magnetic resonance imaging (MRI) parameters and often lack specificity in distinguishing between progression to pathology, such as DLB and PD.[18] Given these limitations, there is a crucial need for novel biomarkers that can stratify iRBD patients based on neurodegeneration severity in targeted brain regions and predict differential progression to DLB or PD. This could guide early targeted neuroprotective interventions, potentially altering the course of the disease.

Free water (FW) quantification from diffusion MRI is a promising approach that quantifies extracellular isotropic diffusion FW to reflect neuroinflammation, edema, and neurodegeneration.[19] This technique enhances traditional diffusion tensor imaging through a bi-compartment model that separates the isotropic diffusion of extracellular FW from the anisotropic, restricted diffusion within tissue.[19] This approach has been applied in various neurodegenerative diseases to detect increases in FW, including PD, where increased FW content has been observed in the posterior region of the substantia nigra (SN),[20–26] a basal ganglia structure strongly associated with parkinsonism and synucleinopathies.[27] FW increase in the SN has been associated with several disease markers and clinical features in PD, including reduced dopamine binding in the striatum[28] and motor features, particularly bradykinesia.[29] FW increases in the basal forebrain (specifically in the nucleus basalis of Meynert [NBM]) of PD patients have also been reported in numerous studies and have been associated with cognitive dysfunction, particularly attention and memory deficits.[30–34] In DLB, similar FW alterations have been observed in the NBM and associated with cholinergic deficits and cognitive decline.[35]

Although FW imaging has been studied in PD and DLB, there are limited data on its application in the prodromal phase, such as iRBD. To date, only three single-center studies have investigated FW changes in the basal forebrain or posterior SN in iRBD patients (≤57 patients) compared to healthy controls.[28,31,36] Although one study did not find changes between iRBD and controls,[36] the others found increased FW content, intermediate between those of controls and PD patients, in the basal forebrain or posterior SN.[28,31] This suggests that FW

increases in iRBD reflect disease progression and early neurodegenerative changes. However, these studies were limited by the absence of longitudinal data and multicentric validation, raising uncertainties regarding the predictive value of FW for differential disease progression in iRBD. Understanding FW changes in the posterior SN and NBM may reveal markers of motor and cognitive pathways associated with phenoconversion from iRBD to PD or DLB.

In this study, we leveraged the largest collection of diffusion MRI scans from video-polysomnography (vPSG)-confirmed iRBD patients and healthy controls, obtained from ongoing prospective, longitudinal cohort studies across five sites worldwide. We processed the diffusion MRI data to extract FW content from the NBM and posterior SN and compared FW content between iRBD patients and controls. We assessed the clinical correlations of FW content in iRBD patients and investigated its predictive capability for determining specific disease progression subtypes, including DLB and PD, or remaining disease-free. Finally, we investigated whether FW predicted phenoconversion independently of structural atrophy in the NBM. We hypothesized that increased FW content in the NBM and posterior SN would be predictive of specific phenoconversion in iRBD patients.

RESEARCH IN CONTEXT

1. **Systematic review**: The authors searched PubMed using "free water," "REM sleep behavior disorder," and "synucleinopathy." FW imaging has emerged as a promising biomarker of neurodegeneration, but previous studies in iRBD were single-center and lacked longitudinal validation.
2. **Interpretation**: This study demonstrates that FW increase in the NBM is a potential biomarker for identifying iRBD patients at high risk of developing DLB. FW in the NBM, but not the SN, predicted conversion to DLB over PD. Increased FW is also associated with lower global cognition in iRBD.
3. **Future directions**: FW in the NBM could help select more homogeneous patient groups for neuroprotective trials targeting early DLB-related pathological mechanisms. It may also serve as a brain-based biological endpoint for assessing neuroprotective efficacy. Future research should integrate FW with other brain biomarkers in early and manifest DLB to better understand its role in disease progression and therapeutic response.

2 | METHODS

2.1 | Sample

This longitudinal, multicenter, prospective study included patients with vPSG-confirmed iRBD and healthy controls who underwent brain MRI, namely, T1-weighted and diffusion-weighted scans. Recruitment was conducted independently at five sites within well-established longitudinal cohorts in sleep and movement disorder clinics. The sites included the Centre for Advanced Research in Sleep Medicine at the Hôpital du Sacré-Coeur de Montréal and The Neuro,[37] Montreal, Canada; the First Faculty of Medicine at Charles University, Prague, Czechia; the Oxford Discovery Cohort, Oxford, United Kingdom; the Movement Disorders Clinic at the Hôpital de la Pitié-Salpêtrière, Paris, France; and the Parkinson's Progression Markers Initiative study.[38]

iRBD was diagnosed according to the International Classification of Sleep Disorders (third edition) criteria, with all patients undergoing one night of vPSG recording.[39] Following diagnosis, patients underwent neurological and cognitive assessments to confirm that RBD was in its isolated phase, iRBD. Patients were excluded if they had already developed an overt neurodegenerative synucleinopathy (DLB, PD, or MSA) at the clinical evaluation closest to the MRI acquisition, as defined by established diagnostic criteria for DLB, PD, and MSA.[40–42] Additional exclusion criteria included any history of brainstem stroke, a diagnosis of epilepsy, epileptiform abnormalities on EEG, antidepressant-triggered RBD, and RBD mimics such as sleepwalking, night terrors, or untreated obstructive sleep apnea. All patients underwent the Montreal Cognitive Assessment (MoCA) to evaluate global cognitive function and the Movement Disorder Society-sponsored Unified Parkinson's Disease Rating Scale (MDS-UPDRS-III) to assess the severity of parkinsonian motor features.[43,44] Patients were monitored prospectively with annual neurological and cognitive examinations to assess any conversion to PD, DLB, or MSA. This study was approved by the research ethics committees at each participating site, with multicentric approval from the CIUSSS du Nord-de-l'Île-de-Montréal and the McGill University Health Centre. All procedures adhered to the ethical standards of the 1964 Declaration of Helsinki and its later amendments. A subset of these participants was studied previously as part of multicentric imaging studies using T1- or diffusion-weighted MRI scans in iRBD.[3,4,45,46]

2.2 | MRI processing

T1- and diffusion-weighted brain MRI scans were acquired at each site using 3T MRI scanners, with acquisition parameters detailed in the Supplementary Material. All MRI scans were visually inspected for artifacts before processing (Figure S1 for workflow). The T1-weighted MRI scans were first processed using FreeSurfer (version 7.1.1), following established methods to segment the cortical and subcortical structures.[3] The segmented maps and surfaces from FreeSurfer were then combined with the diffusion-weighted images and corresponding bval and bvec files as inputs to the TractoFlow-Atlas-Based Segmentation (TractoFlow-ABS) pipeline[47] run on high-performance computing (HPC) resources. TractoFlow-ABS is an automated diffusion MRI processing pipeline designed to perform artifact removal, preprocessing, and tractography for robust, large-scale quantitative analyses.[47] Key parameters for diffusion imaging processing included both

single-shell and multishell data, and FW estimation was performed using single-shell data. Fiber response functions were set adaptatively, and tractography was conducted using local probabilistic tracking. Seeding was applied at the white matter/gray matter interface with 20 seeds per voxel. Spherical harmonics were set to order 6 for datasets with fewer than 32 gradient directions and to order 8 otherwise. FW fractions, ranging from 0 to 1 per voxel, were calculated using the Free-Water Flow tool[19,48–50] and Python 3.8 with AMICO wheels on HPC resources. Key parameters included an axial diffusivity of 0.001 in the corpus callosum, a mean diffusivity of 0.0025 in the ventricles, and a radial diffusivity range of 0.0001 to 0.0065, with specific regularization settings.

To extract FW content, regions of interest (ROIs) were aligned with the Montreal Neurological Institute (MNI152) template space. Basal forebrain ROIs were derived using a probabilistic atlas from *post mortem* data in the JuBrain Anatomy toolbox (version 2.2) with Mesulam's nomenclature. Two distinct basal forebrain ROIs were selected, namely, the left and right NBM, as the primary ROIs. SN ROIs were defined using an isotropic 2-mm box in MarsBar, with coordinates set for left posterior SN ($x = -11, y = -21, z = -13$) and right posterior SN ($x = 11, y = -21, z = -13$) as target areas, as well as left anterior SN ($x = -9, y = -15, z = -13$) and right anterior SN ($x = 9, y = -15, z = -13$) as additional control areas (Figure S1).

For mask registration, T1-weighted images were further processed using the CAT12 toolbox in SPM12 (release 6906)[51] under MATLAB R2018B to produce whole-brain warped and modulated maps per patient. This step involved segmentation into tissue classes, bias correction for intensity nonuniformity, and non-linear transformation to MNI template space. Transformation maps for aligning ROIs to patient space were generated using Advanced Normalization Tools with customized codes. This procedure involved registering each mask to the T1-warped image from TractoFlow using the antsApplyTransforms tool with the NearestNeighbor function. MarsBar-defined ROIs were similarly transformed. Customized scripts were then used to extract mean FW values for each ROI. FW values close to 0 indicate restricted water movement within tissue, while values near 1 reflect free diffusion in the extracellular space, indicating neuroinflammation.

To determine whether FW content in the basal forebrain predicted phenoconversion independently of regional atrophy, we also extracted gray matter volume from the same NBM regions in all participants. The NBM ROIs were identical to those used for FW extraction. Masks for the left and right NBM were co-registered and resliced to the MNI152 template using SPM12. Gray matter volume estimates (in cubic millimeters [mm^3]) were then extracted from unsmoothed, modulated gray matter maps using the "get_totals" script. Since volume scales with head size, total intracranial volume was extracted for each participant, and all volume measures were normalized by dividing each regional volume by the corresponding total intracranial volume.

2.3 | Statistical analyses

To address variability in multicenter data collected using different scanners, the ComBat harmonization algorithm was applied to the FW values to correct for scanner-related effects.[52,53] This method has been validated in neuroimaging studies, including diffusion MRI,[54] and enables robust site-level adjustment while preserving biological variability.

The primary outcome variable was phenoconversion status in iRBD patients, categorized into three groups: iRBD converters to DLB, iRBD converters to PD, and iRBD non-converters (disease-free at last follow-up). For cross-sectional analyses, group comparisons of normally distributed demographic, clinical, and imaging variables (FW and volume) were performed using independent sample *t*-tests for continuous variables and chi-squared tests for categorical variables. Non-normally distributed variables were assessed using the Mann–Whitney U test. Correlations between FW values in the NBM and posterior SN and clinical features (MoCA and MDS-UPDRS-III) were assessed using Pearson's *r*, followed by partial correlations controlling for age and sex. Hemispheric differences in correlation strength were assessed using Hotelling's *t*-test and Zou's confidence interval method.

For longitudinal phenoconversion analyses, multinomial logistic regression was used to evaluate the predictive value of FW measures on phenoconversion odds. Model 1 tested FW in the NBM, Model 2 tested FW in the posterior SN, and Model 3 included both regions simultaneously, adjusting for age and sex in all models. To confirm regional specificity, these models were repeated using the FW values from the anterior SN as a control region. To examine whether FW predicted phenoconversion independently of structural atrophy, we also tested whether NBM volume predicted conversion type and whether FW predicted phenoconversion when both FW and NBM volume were added in the same regression model.

To investigate time to phenoconversion, Kaplan–Meier survival analyses were performed. The MRI acquisition date was considered time 0, and follow-up time was computed as the interval to the latest clinical evaluation (or date of phenoconversion). Patients were stratified into high and low FW groups based on the median value within the iRBD sample. Log-rank tests were used to assess group differences in survival. Additional Kaplan–Meier curves were generated for specific conversion types (DLB vs PD vs non-converters). Cox proportional hazards regression models were used to assess whether FW content predicted time to phenoconversion independently from age, sex, and clinical measurements. All FW values were *z*-scored to standardize interpretation of odds ratios (ORs) and hazard ratios. Likelihood ratio tests were used to evaluate model fit. All statistical analyses were conducted using IBM SPSS Statistics (version 29.0) and RStudio (version 2023.06.2).

3 | RESULTS

3.1 | Participants

The multicenter iRBD cohort initially included 592 participants, comprising 289 vPSG-confirmed iRBD patients and 303 controls, each with both T1- and diffusion-weighted brain MRI scans acquired across five centers as part of this prospective study (Figure 1). The cohort included 159 participants from Montreal, 140 from Prague, 132 from

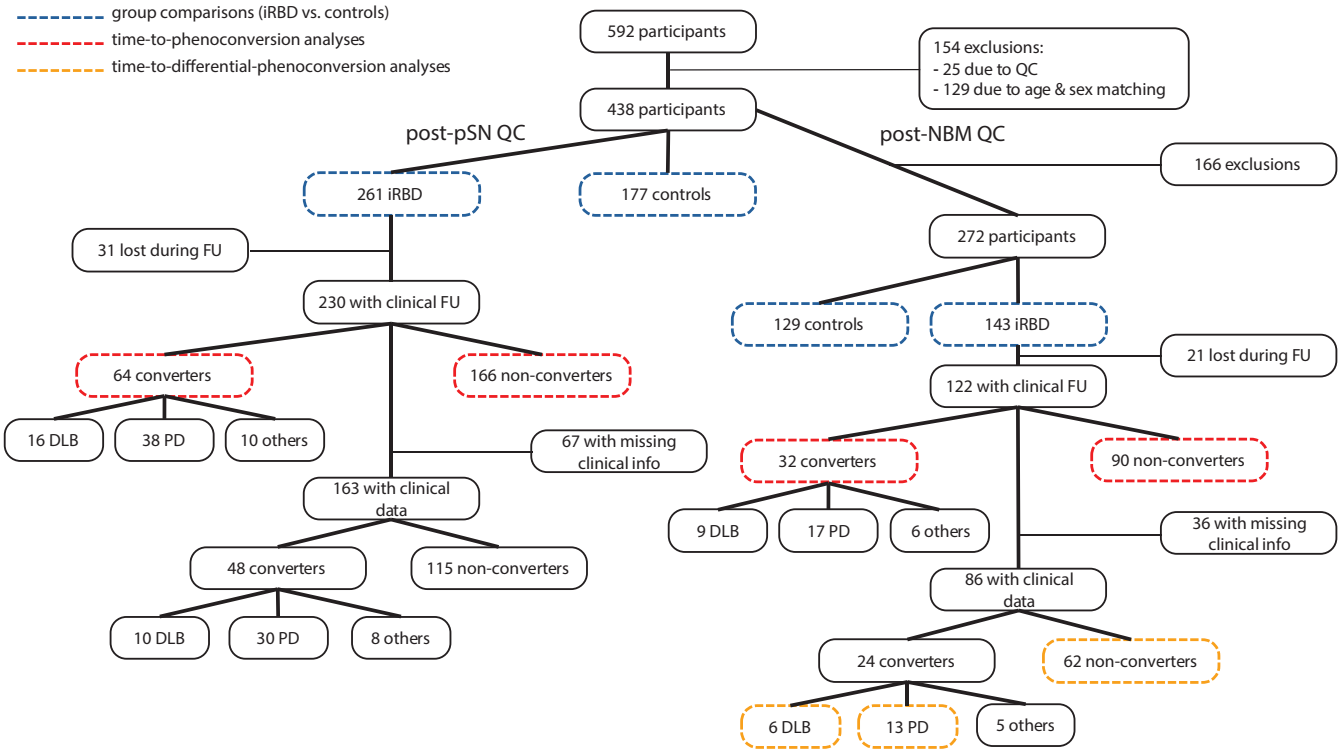

FIGURE 1 Flowchart illustrating participant selection and inclusion for NBM and pSN analyses. Participants were excluded based on quality control, demographic matching, and availability of clinical measures. Time-to-differential-phenoconversion analyses were only done for the NBM, as only FW in the NBM was retained as a significant predictor when used alongside the pSN. DLB, dementia with Lewy bodies; FW, free water; iRBD, isolated REM sleep behavior disorder; NBM, nucleus basalis of Meynert; PD, Parkinson's disease; pSN, posterior substantia nigra; QC, quality control.

Oxford, 107 from Paris, and 54 from the Parkinson's Progression Markers Initiative study. All scans successfully passed initial diffusion MRI processing; however, 25 were excluded during visual quality control due to misregistration, resulting in 567 scans eligible for analysis. To ensure comparability between iRBD and control groups, 129 scans were excluded for statistical matching on age and sex. Most exclusions occurred in the control group, with 126 controls and 28 iRBD patients excluded. All MRI processing and FW estimation were performed prior to matching to prevent post hoc quality control from introducing imbalances. A total of 438 participants (261 iRBD patients, 177 controls) were therefore retained for analyses involving the posterior SN, with no further exclusions, as all scans showed satisfactory alignment.

In this sample, iRBD patients had a mean age of 66.3 years (SD: 6.5), with 32 (12%) identifying as female. The mean MoCA score was 25.4 (SD: 3.0), and the mean score on the MDS-UPDRS-III was 6.4 (SD: 5.5) (Table 1). iRBD patients had significantly lower MoCA scores and higher MDS-UPDRS-III scores compared to controls ($p < 0.001$). As expected, based on the initial group compositions, demographic comparisons between included and excluded participants reflected the effects of matching. Excluded controls were significantly younger (58.1 years, $p < 0.001$) and more often female (72%, $p < 0.001$), while excluded iRBD patients were older (73.9 years, $p < 0.001$). No significant differences were observed in MoCA scores ($p = 0.24$), MDS-UPDRS-III ($p = 0.91$), or sex ($p = 0.20$) among excluded versus included iRBD patients. Following a strict quality control procedure for the NBM due to its anatomical proximity to cerebrospinal fluid (CSF), which can contaminate FW estimates, 272 MRI scans were retained for this region, comprising 143 iRBD patients and 129 controls with similar age ($p = 0.62$) and sex distribution ($p = 0.13$). Patients with iRBD included in the NBM ($n = 143$) and posterior SN analyses ($n = 261$) did not differ in age ($p = 0.33$), sex distribution ($p = 0.73$), MoCA scores ($p = 0.40$), and MDS-UPDRS-III scores ($p = 0.50$).

3.2 | Free water does not distinguish between iRBD patients and controls

We first investigated whether FW content in the NBM and posterior SN differed between the overall group of iRBD patients and controls. In the NBM, the mean FW value was 0.295 (SD: 0.07) for patients and 0.291 (SD: 0.07) for controls, with a non-significant mean difference of −0.004 (95% confidence interval [CI]: −0.02 to 0.01; $p = 0.61$) (Figure 2, Tables 1 and S1 for center-specific demographic and clinical varibles). Similarly, in the bilateral posterior SN, the mean FW value was 0.216 (SD: 0.10) for patients and 0.221 (SD: 0.10) for controls, with a non-significant mean difference of 0.006 (95% CI: −0.01 to 0.02; $p = 0.54$) (Figure 2 and Table 1). Furthermore, no significant difference in FW

TABLE 1 Demographic, clinical, and imaging variables of iRBD patients and controls.

Variables	iRBD patients	Controls	*p* value	Converters	Non-converters	*p* value
NBM analyses						
Age at MRI, years	65.6 ± 6.1	66.00 ± 6.4	0.62[a]	65.0 ± 4.8	65.3 ± 6.7	0.82[a]
Sex, *n* (% male)	123 (86%)	102 (79%)	0.13[b]	29 (91%)	78 (87%)	0.13[b]
MDS-UPDRS-III	6.1 ± 5.5	4.3 ± 6.2	**<0.001**[c]	7.1 ± 6.5	5.7 ± 5.2	0.33[c]
MoCA	25.1 ± 3.3	26.6 ± 2.5	**<0.001**[c]	24.3 ± 3.2	25.7 ± 3.0	**0.025**[c]
FW NBM, bilateral	0.295 ± 0.07	0.291 ± 0.07	0.61[a]	0.327 ± 0.06	0.282 ± 0.06	**<0.001**[a]
FW NBM, left	0.321 ± 0.07	0.314 ± 0.08	0.45[a]	0.353 ± 0.07	0.308 ± 0.07	**0.003**[a]
FW NBM, right	0.265 ± 0.07	0.266 ± 0.07	0.96[a]	0.296 ± 0.06	0.253 ± 0.07	**0.003**[a]
NBM volume,[d] bilateral	$1.95\times10^{-4}\pm1.80\times10^{-5}$	$2.02\times10^{-4}\pm1.56\times10^{-5}$	**<0.001**[a]	$1.87\times10^{-4}\pm1.60\times10^{-5}$	$1.98\times10^{-4}\pm1.84\times10^{-5}$	**<0.001**[a]
NBM volume,[d] left	$9.82\times10^{-5}\pm1.02\times10^{-5}$	$1.02\times10^{-4}\pm8.93\times10^{-6}$	**<0.001**[a]	$9.45\times10^{-5}\pm8.82\times10^{-6}$	$9.97\times10^{-5}\pm1.06\times10^{-5}$	**<0.001**[a]
NBM volume,[d] right	$9.71\times10^{-5}\pm8.91\times10^{-6}$	$1.00\times10^{-4}\pm8.20\times10^{-6}$	**<0.001**[a]	$9.28\times10^{-5}\pm8.31\times10^{-6}$	$9.87\times10^{-5}\pm8.90\times10^{-6}$	**<0.001**[a]
SN analyses						
Age at MRI, years	66.3 ± 6.5	66.1 ± 6.6	0.79[a]	66.4 ± 6.0	65.8 ± 6.8	0.52[a]
Sex, *n* (% male)	229 (88%)	145 (82%)	0.09[b]	58 (91%)	147 (89%)	0.65[b]
MDS-UPDRS-III	6.4 ± 5.5	4.0 ± 6.1	**<0.001**[c]	6.9 ± 5.7	6.2 ± 5.6	0.28[c]
MoCA	25.4 ± 3.0	26.7 ± 2.4	**<0.001**[c]	25.0 ± 3.0	25.9 ± 2.8	**0.028**[c]
FW pSN, bilateral	0.216 ± 0.10	0.221 ± 0.10	0.54[a]	0.231 ± 0.08	0.208 ± 0.10	0.09[a]
FW pSN, left	0.214 ± 0.12	0.217 ± 0.11	0.80[a]	0.237 ± 0.11	0.202 ± 0.11	**0.038**[a]
FW pSN, right	0.218 ± 0.10	0.227 ± 0.11	0.40[a]	0.226 ± 0.09	0.213 ± 0.11	0.40[a]
FW aSN, bilateral	0.150 ± 0.11	0.148 ± 0.11	0.88[a]	0.160 ± 0.09	0.144 ± 0.11	0.30[a]
FW aSN, left	0.147 ± 0.13	0.149 ± 0.13	0.92[a]	0.153 ± 0.12	0.140 ± 0.13	0.48[a]
FW aSN, right	0.152 ± 0.12	0.148 ± 0.12	0.70[a]	0.167 ± 0.12	0.147 ± 0.12	0.28[a]

Note: Continuous data are presented as mean ± SD. Bold values represent significant differences.

Abbreviations: aSN, anterior substantia nigra; FW, free water; iRBD, isolated REM sleep behavior disorder; MDS, Movement Disorder Society; MoCA, Montreal Cognitive Assessment; NBM, nucleus basalis of Meynert; pSN, posterior substantia nigra; SD, standard deviation; UPDRS-III, Unified Parkinson's Disease Rating Scale, motor scale.

[a]Student's *t*-test.

[b]Chi-squared test.

[c]Mann–Whitney U test.

[d]Volume measures were normalized for total intracranial volume.

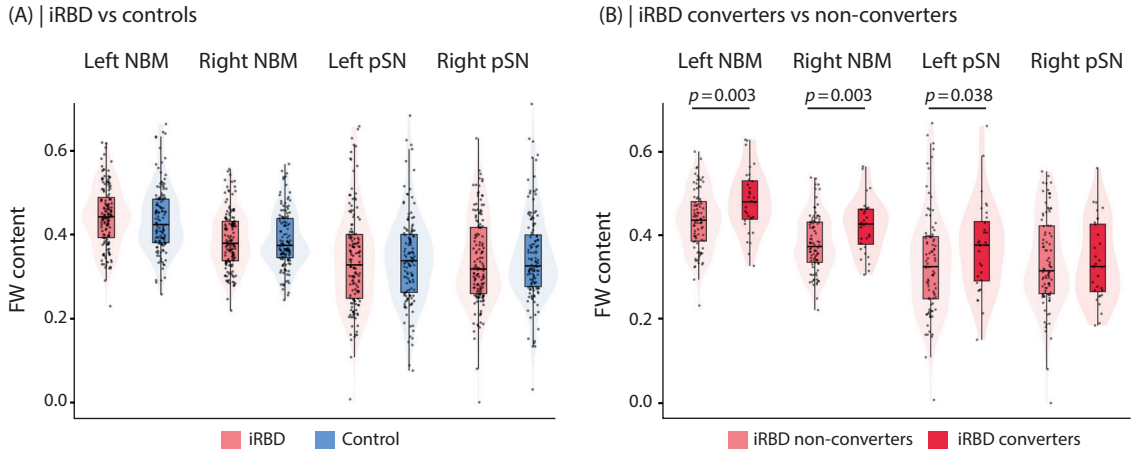

FIGURE 2 FW levels in iRBD patients and controls. (A) Box plots and violin plots showing distribution of FW content in NBM and pSN for iRBD patients (red) and healthy controls (blue). FW content is presented after harmonization for scanner effects, with values standardized to positive values for visualization purposes. No significant differences were observed between groups in either region. (B) Box plots and violin plots showing distribution of FW content in NBM and posterior SN for iRBD converters (dark red) and non-converters (light red). FW content in NBM and pSN was significantly increased in iRBD converters compared to non-converters. FW, free water; iRBD, isolated REM sleep behavior disorder; NBM, nucleus basalis of Meynert; pSN, posterior substantia nigra.

content was observed between groups when the NBM and posterior SN were separated into left and right hemispheres or when analyzing the anterior SN as a control region (Figure 2, Table 1, and Figure S2). Controls excluded after processing and matching had lower FW in the NBM (0.24, $p < 0.001$), while excluded iRBD patients had higher NBM FW (0.37, $p = 0.013$) (i.e., no bias introduced towards research hypothesis), with no significant differences in the posterior SN or anterior SN ($p > 0.05$).

3.3 | Free water in NBM is associated with cognitive decline

We examined whether FW content in the NBM and posterior SN was correlated with MoCA and MDS-UPDRS-III scores in iRBD patients. We observed a significant negative correlation between FW in the NBM and MoCA scores in iRBD patients, with increased FW content associated with decreased MoCA scores ($r = -0.25$, $p = 0.004$) (Figure 3). This association was significant in both hemispheres, with a correlation of $r = -0.27$ ($p = 0.002$) in the left hemisphere and $r = -0.18$ ($p = 0.036$) in the right hemisphere. The strength of the correlation between FW and MoCA did not significantly differ between hemispheres (coefficient difference = −0.08, 95% CI: −0.23 to 0.06, $p = 0.23$). However, after adjusting for age and sex, the association remained significant only for the left NBM. In contrast, there were no significant correlations between FW content in either the NBM or the posterior SN and MDS-UPDRS-III scores in iRBD patients ($p = 0.45$ for NBM, $p = 0.58$ for posterior SN). Additionally, FW content in the posterior SN did not show a significant correlation with MoCA scores in iRBD patients ($p = 0.59$), nor were there significant correlations with FW in the control group (all $p > 0.05$).

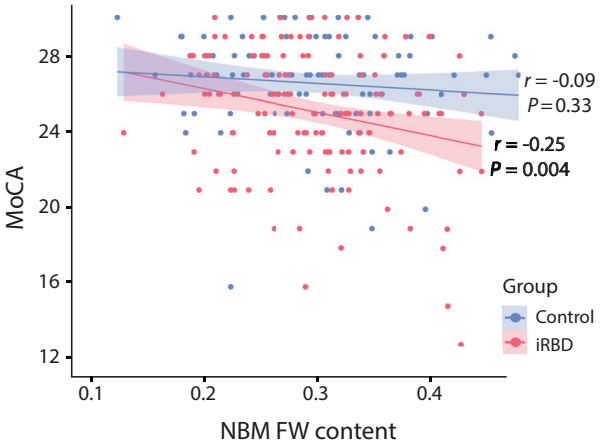

FIGURE 3 Scatter plot showing relationship between FW content in NBM and MoCA scores in iRBD patients (red) and healthy controls (blue). The shaded areas represent the 95% confidence intervals for the regression lines. In iRBD, higher FW content in the NBM was significantly associated with lower MoCA scores; no significant correlation was observed in controls. FW, free water; iRBD, isolated REM sleep behavior disorder; MoCA, Montreal Cognitive Assessment; NBM, nucleus basalis of Meynert.

3.4 | Increased FW is associated with higher risk of phenoconversion in iRBD

To assess whether FW may be associated with disease progression in iRBD, we compared FW content in the NBM and posterior SN between iRBD patients who progressed to an overt synucleinopathy during follow-up versus those who remained disease-free. Of the 261 patients, 31 (12%) were lost to follow-up, resulting in a sample of 230 iRBD patients followed longitudinally. There were no

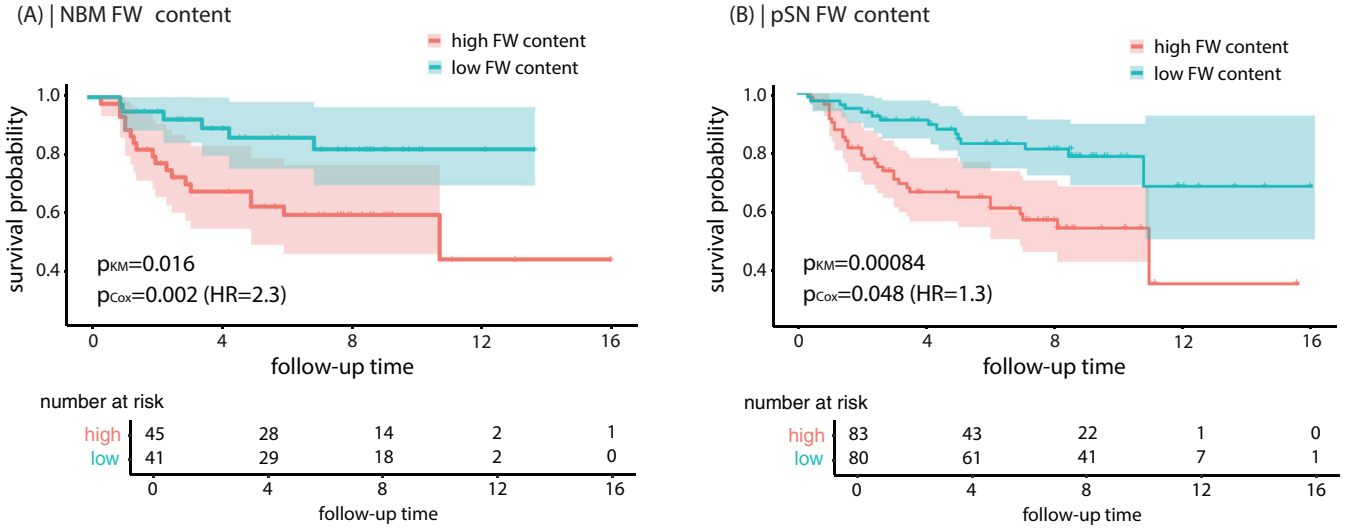

FIGURE 4 Kaplan–Meier survival curves showing survival probabilities (i.e., remaining disease-free at the latest clinical follow-up compared to receiving a diagnosis of neurodegenerative disease) over time based on FW content in (A) NBM and (B) the pSN. High FW content based on median FW level is represented in red and low FW content is represented in blue. Shaded areas indicate 95% confidence intervals for each group. FW, free water; HR, hazard ratio; iRBD, isolated REM sleep behavior disorder; KM, Kaplan-Meier; NBM, nucleus basalis of Meynert; pSN, posterior substantia nigra.

significant differences in FW values between patients lost to follow-up and those followed longitudinally for the NBM (p = 0.56), posterior SN (p = 0.45), anterior SN (p = 0.55), or in age (p = 0.06), sex (p = 0.06), and MDS-UPDRS-III score (p = 0.38). However, a significant difference was observed in MoCA scores (p = 0.002), with patients lost to follow-up showing lower cognitive performance compared to those retained (23.7 vs 25.7, p = 0.002). Patients were followed for a median of 8.4 years (range: 4 months to 16 years). At their latest clinical examination, 64 (28%) patients had converted to a neurodegenerative disease (converters), while 166 (72%) remained disease-free (non-converters). There were no significant differences between converters and non-converters regarding age at MRI scan (p = 0.52), sex (p = 0.65), and MDS-UPDRS-III score (p = 0.28) (Table 1). However, iRBD converters had lower scores on the MoCA (p = 0.028) (Table 1).

When stratifying iRBD patients by phenoconversion status, we found significant differences in FW content between converters and non-converters. iRBD converters exhibited higher FW values bilaterally in the NBM compared to non-converters, with a mean difference of −0.044 ± 0.013 (95% CI: −0.070 to −0.019, $p < 0.001$) (Table 1 and Figure 2). This increase was significant in both the left (mean difference: −0.045 ± 0.015, 95% CI: −0.074 to −0.016, p = 0.003) and right NBM (mean difference: −0.042 ± 0.038, 95% CI: −0.069 to −0.015, p = 0.003) (Table 1). In the posterior SN, iRBD converters showed increased FW only on the left side (mean difference: −0.034 ± 0.017, 95% CI: −0.068 to −0.002, p = 0.038) (Table 1 and Figure 2). To verify the specificity of these findings, we further assessed FW content in the anterior SN as a control region and did not find significant changes between groups (p = 0.48 on the left and p = 0.28 on the right) (Table 1 and Figure S3). When comparing iRBD converters and non-converters to controls, we found that iRBD non-converters had similar FW content in the NBM (p = 0.34) and posterior SN (p = 0.23) compared to controls.

Of the 230 iRBD patients with follow-up, 67 had missing clinical information for time-to-event analyses, resulting in a post-quality-controlled sample of 163 patients (48 converted) for posterior SN analyses and 86 patients (24 converted) for NBM analyses. Kaplan–Meier survival analyses were conducted to assess whether FW content in the NBM and posterior SN predicted time to phenoconversion (in years) in iRBD (Table S2 for demographics). Patients were dichotomized into high and low FW groups based on the median FW content across the iRBD cohort. Survival curves revealed that higher FW content in both the NBM (p = 0.016) and posterior SN (p = 0.00084) was associated with a significantly increased risk of phenoconversion over time (Figure 4). When adjusting for age and sex using Cox proportional hazards regression models, increased FW in both regions remained significant predictors of phenoconversion. Specifically, higher FW in the NBM was associated with a two-fold increased risk of conversion (HR = 2.35, 95% CI: 1.36 to 4.05, p = 0.002) and increased FW in the posterior SN was linked to a 1.3-fold increased conversion risk (HR = 1.33, 95% CI: 1.00 to 1.77, p = 0.048) (Table S3). Among patients with high FW content in the NBM, 80% remained disease-free at 2 years compared to 95% of those with low FW content; survival dropped to 68% at 4 years and 60% at 8 years (Figure 4A). Similarly, for the posterior SN, 79% of patients with high FW content were disease-free at 2 years (vs 94% with low FW), 67% at 4 years, and 58% at 8 years (Figure 4B). However, importantly, Cox regression models including FW in both the NBM and posterior SN, along with age and sex, revealed that only NBM FW was a significant predictor of phenoconversion in iRBD (HR = 2.30, 95% CI: 1.33 to 3.98, p = 0.003), and not posterior SN (HR = 1.12, 95% CI: 0.74 to 1.69, p = 0.58) (Table

S3). Furthermore, when adding both MoCA and MDS-UPDRS-III to the previously mentioned predictors, only NBM FW was a significant predictor of phenoconversion in iRBD (HR = 2.57, 95% CI: 1.32 to 4.98, $p = 0.005$) (Table S3). This indicates that while increased FW content in the NBM or posterior SN was associated with a higher risk of phenoconversion in iRBD, only FW in the NBM predicted this risk when considered simultaneously.

3.5 | Free water in NBM predicts DLB over PD in iRBD

We next investigated whether FW content in the NBM and posterior SN could predict specific phenoconversion pathways (i.e., DLB vs PD) in iRBD. Among the 230 iRBD patients with longitudinal follow-up, 10 (4%) converted to other neurodegenerative syndromes (e.g., MSA or pure autonomic failure) and were excluded, yielding a sample of 220 iRBD patients. These were classified as converters to DLB ($n = 16$), converters to PD ($n = 38$), or non-converters ($n = 166$). Model 1 (logistic regression), testing FW in the NBM while adjusting for age and sex, revealed that higher FW content significantly predicted conversion to DLB compared to remaining disease-free ($\beta = 1.94$, $p < 0.001$), with an OR of 6.92 (95% CI: 2.28 to 21.04) per one-SD increase in NBM FW (Table 2). In contrast, NBM FW did not significantly predict conversion to PD ($\beta = 0.51$, $p = 0.11$, OR = 1.67, 95% CI: 0.89 to 3.15). However, FW in the NBM did differentiate DLB from PD converters ($\beta = 1.42$, $p = 0.019$), with an OR of 4.14 (95% CI: 1.26 to 13.55), suggesting selective sensitivity to DLB progression (Table 2).

Model 2, testing FW in the posterior SN alone, along with age and sex, was not significant ($p > 0.27$) (Table 2). To rule out sample composition as a confounding factor, we repeated this posterior SN model using the same subset of iRBD patients as included in the NBM analysis. In this restricted sample, FW in the posterior SN also did not predict conversion to DLB ($p = 0.36$) or PD ($p = 0.75$). Model 3, which included FW in both the NBM and posterior SN, along with age and sex, confirmed that NBM FW predicted phenoconversion to DLB versus remaining disease-free ($\beta = 1.90$, $p < 0.001$, OR = 6.69, 95% CI: 2.22 to 20.19), as well as DLB versus PD ($\beta = 1.39$, $p = 0.021$, OR = 4.00, 95% CI: 1.23 to 12.99) (Table 2). FW in the anterior SN (control region) was not associated with phenoconversion in any of the analyses (Table S4). In terms of time-to-event analyses (Table S5 for demographics), Kaplan–Meier survival curves further indicated that iRBD patients with higher FW in the NBM had a significantly greater likelihood of converting to DLB over time compared to remaining disease-free ($p = 0.023$), with a trend also observed for conversion to PD compared to remaining disease-free ($p = 0.051$) (Figure 5). However, in Cox proportional hazards regression models adjusting for age and sex, only FW in the NBM remained a significant predictor of DLB conversion (HR = 8.22, 95% CI: 2.00 to 33.80, $p = 0.003$), while association with PD was no longer significant (HR = 1.59, 95% CI: 0.80 to 3.18, $p = 0.19$) (Tables S6 and S7). This indicates that increased FW content in the NBM is a specific marker of DLB phenoconversion in iRBD.

3.6 | NBM FW predicts conversion independently of atrophy

Next, we investigated whether FW in the NBM provided additional predictive value over structural atrophy for identifying iRBD patients at risk of phenoconversion. Mean NBM volume (normalized for head size) was significantly lower in iRBD patients ($1.95 \times 10^{-4} \pm 1.80 \times 10^{-5}$) compared to controls ($2.02 \times 10^{-4} \pm 1.56 \times 10^{-5}$), with a mean difference of 6.62×10^{-6} (95% CI: 3.36×10^{-6} to 9.88×10^{-6}, $p < 0.001$) (Table 1). Among iRBD patients, converters had lower NBM volume ($1.87 \times 10^{-4} \pm 1.60 \times 10^{-5}$) than non-converters ($1.98 \times 10^{-4} \pm 1.84 \times 10^{-5}$), with a mean difference of 1.11×10^{-5} (95% CI: 5.93×10^{-6} to 1.62×10^{-5}, $p < 0.001$) (Table 1). Lower NBM volume was significantly associated with increased odds of converting to DLB compared to remaining disease-free ($\beta = -0.77$, $p = 0.044$, OR = 0.46, 95% CI: 0.22 to 0.98), but not to PD ($\beta = -0.35$, $p = 0.15$), and did not distinguish DLB from PD (β = -0.42, $p = 0.30$) (Table 3). When both NBM FW and NBM volume were entered into the same model, FW in the NBM was a significant predictor of DLB conversion ($\beta = 2.01$, $p = 0.035$, OR = 7.45, 95% CI = 1.15 to 48.24), while NBM volume was no longer significant ($\beta = -0.73$, $p = 0.16$) (Table 3). These findings demonstrate that FW in the NBM is a more sensitive and specific marker of phenoconversion to DLB than structural atrophy.

4 | DISCUSSION

In this study, we leveraged the largest collection of diffusion MRI scans from vPSG-confirmed iRBD patients and healthy controls to investigate whether FW content in the NBM and posterior SN predicted phenoconversion trajectories in iRBD. Our results demonstrate that changes in FW within these regions are associated with disease progression toward synucleinopathies. Although no significant group differences were observed between iRBD patients and controls in either the NBM or posterior SN overall, stratification by phenoconversion status revealed that increased FW content in both regions was present among converters. Importantly, increased FW in the NBM was selectively associated with conversion to DLB, rather than PD or remaining disease-free, indicating it may serve as an early marker of DLB-specific progression. Although NBM volume was also significantly reduced in iRBD patients and in converters, only FW remained a significant predictor of DLB conversion when both measures were entered into the same model. This suggests that FW in the NBM captures disease-relevant structural changes beyond atrophy, offering a more sensitive biomarker of phenoconversion risk in iRBD.

Several studies have shown that increases in FW occur in overt synucleinopathies, reflecting neuroinflammation, gliosis, axonal damage, and cell loss.[55] In PD, FW increases in the posterior SN and basal forebrain have been associated with motor features, attentional deficits, and memory impairments.[20,28–30] In DLB, FW increases in the NBM have been associated with cholinergic dysfunction and cognitive decline.[35] Importantly, these FW changes can be observed even in the

TABLE 2 Logistic regression models of FW predicting phenoconversion in iRBD.

	DLB vs disease-free[a]			PD vs disease-free[a]			DLB vs PD[b]		
Model Terms	**Coefficient (SE)**	***p* value**	**OR (95% CI)**	**Coefficient (SE)**	***p* value**	**OR (95% CI)**	**Coefficient (SE)**	***p* value**	**OR (95% CI)**
Model 1: NBM FW content									
FW[c]	1.94 (0.57)	**<0.001**	6.92 (2.28; 21.04)	0.51 (0.32)	0.11	1.67 (0.89; 3.15)	1.42 (0.61)	**0.019**	4.14 (1.26; 13.55)
Age	−0.17 (0.08)	**0.032**	0.85 (0.73; 0.99)	−0.003 (0.05)	0.95	0.10 (0.91; 1.10)	−0.17 (0.09)	0.06	0.85 (0.72; 1.00)
Sex[d]	1.74 (1.34)	0.19	5.72 (0.41; 79.21)	−0.60 (1.10)	0.59	0.55 (0.06; 4.76)	2.34 (1.67)	0.16	10.41 (0.40; 272.97)
Intercept	7.38 (4.79)	0.12	-	−1.51 (3.23)	0.64	-	8.89 (5.35)	0.10	-
Model 2: pSN FW content									
FW[c]	0.23 (0.26)	0.37	1.26 (0.76; 2.09)	0.20 (0.18)	0.27	1.22 (0.86; 1.72)	0.03 (0.30)	0.91	1.04 (0.58; 1.85)
Age	0.01 (0.04)	0.90	1.01 (0.93; 1.09)	0.04 (0.03)	0.22	1.04 (0.98; 1.10)	−0.03 (0.05)	0.52	0.97 (0.88; 1.06)
Sex[d]	0.45 (0.68)	0.50	1.58 (0.42; 5.94)	−0.96 (0.76)	0.21	0.38 (0.09; 1.69)	1.42 (0.97)	0.14	4.13 (0.62; 27.65)
Intercept	−3.00 (2.70)	0.27	-	−4.01 (1.95)	**0.040**	-	1.02 (3.18)	0.75	-
Model 3: NBM and pSN FW content									
FW NBM[c]	1.90 (0.56)	**<0.001**	6.69 (2.22; 20.19)	0.52 (0.32)	0.11	1.67 (0.89; 3.15)	1.39 (0.60)	**0.021**	4.00 (1.23; 12.99)
FW pSN[c]	0.20 (0.39)	0.60	1.23 (0.57; 2.62)	0.08 (0.25)	0.75	1.09 (0.66; 1.77)	0.12 (0.43)	0.78	1.13 (0.49; 2.63)
Age	−0.17 (0.08)	**0.033**	0.85 (0.73; 0.99)	−0.004 (0.05)	0.94	0.10 (0.90; 1.10)	−0.164 (0.086)	0.06	0.85 (0.72; 1.01)
Sex[d]	1.72 (1.34)	0.20	5.60 (0.41; 76.84)	−0.58 (1.10)	0.56	0.56 (0.06; 4.85)	2.30 (1.66)	0.17	10.02 (0.39; 260.32)
Intercept	7.41 (4.82)	0.12	-	−1.46 (3.25)	0.65	-	8.88 (5.38)	0.10	-

Abbreviations: CI, confidence interval; DLB, dementia with Lewy bodies; FW, free water; iRBD, isolated REM sleep behavior disorder; MoCA, Montreal Cognitive Assessment; NBM, nucleus basalis of Meynert; OR, odds ratio; PD, Parkinson's disease; pSN, posterior substantia nigra; SE, standard error.

[a]Disease-free was used as reference category.

[b]PD was used as reference category.

[c]FW levels were entered as *z*-scores to improve interpretability of a one-SD unit change in FW.

[d]Sex was coded as female = 0 and male = 1.

TABLE 3 Logistic regression models of NBM volume predicting phenoconversion in iRBD.

	DLB vs disease-free[a]			PD vs disease-free[a]			DLB vs PD[b]		
Model Terms	**Coefficient (SE)**	***p* value**	**OR (95% CI)**	**Coefficient (SE)**	***p* value**	**OR (95% CI)**	**Coefficient (SE)**	***p* value**	**OR (95% CI)**
NBM volume									
Volume[c,d]	−0.77 (0.38)	**0.044**	0.46 (0.22; 0.98)	−0.35 (0.25)	0.15	0.70 (0.43; 1.14)	−0.42 (0.41)	0.304	1.52 (0.66; 1.46)
Age	−0.01 (0.06)	0.82	0.99 (0.87; 1.12)	0.02 (0.04)	0.69	1.02 (0.94; 1.10)	−0.03 (0.07)	0.65	0.97 (0.85; 1.11)
Sex[e]	1.26 (0.81)	0.12	3.53 (0.72; 17.38)	−0.78 (0.83)	0.35	0.46 (0.09; 2.32)	2.04 (1.05)	0.051	7.69 (0.99; 59.82)
Intercept	−0.69 (4.09)	0.87	-	−0.70 (2.76)	0.80	-	0.011 (4.49)	0.10	-
NBM volume and FW									
Volume[c,d]	−0.73 (0.52)	0.16	0.48 (0.18; 1.33)	−0.23 (0.35)	0.51	0.79 (0.40; 1.58)	−0.50 (0.55)	0.37	0.61 (0.21; 1.80)
FW[c]	2.01 (0.95)	**0.035**	7.45 (1.15; 48.24)	0.12 (0.47)	0.81	1.12 (0.45; 2.79)	1.89 (1.0)	0.058	6.64 (0.94; 47.05)
Age	−0.21 (0.13)	0.12	0.81 (0.62; 1.06)	0.01 (0.08)	0.90	1.01 (0.87; 1.18)	−0.22 (0.14)	0.13	0.80 (0.61; 1.06)
Sex[e]	2.55 (1.78)	0.15	12.75 (0.39; 415.99)	−1.08 (1.21)	0.38	0.34 (0.03; 3.75)	3.63 (2.01)	0.71	37.67 (0.73; 1939.51)
Intercept	9.99 (7.89)	0.21	-	0.20 (5.15)	0.97	-	9.79 (8.47)	0.25	-

Abbreviations: CI, confidence intervals; DLB, dementia with Lewy bodies; FW, free water; iRBD, isolated REM sleep behavior disorder; MoCA = Montreal Cognitive Assessment; NBM, nucleus basalis of Meynert; OR, odds ratio; PD, Parkinson's disease; pSN, posterior substantia nigra; SE, standard error.

[a]Disease-free was used as reference category.

[b]PD was used as reference category.

[c]FW and volume were entered as z-scores to improve interpretability of a one-SD unit change.

[d]Volume measures were normalized for total intracranial volume.

[e]Sex was coded as female = 0 and male = 1.

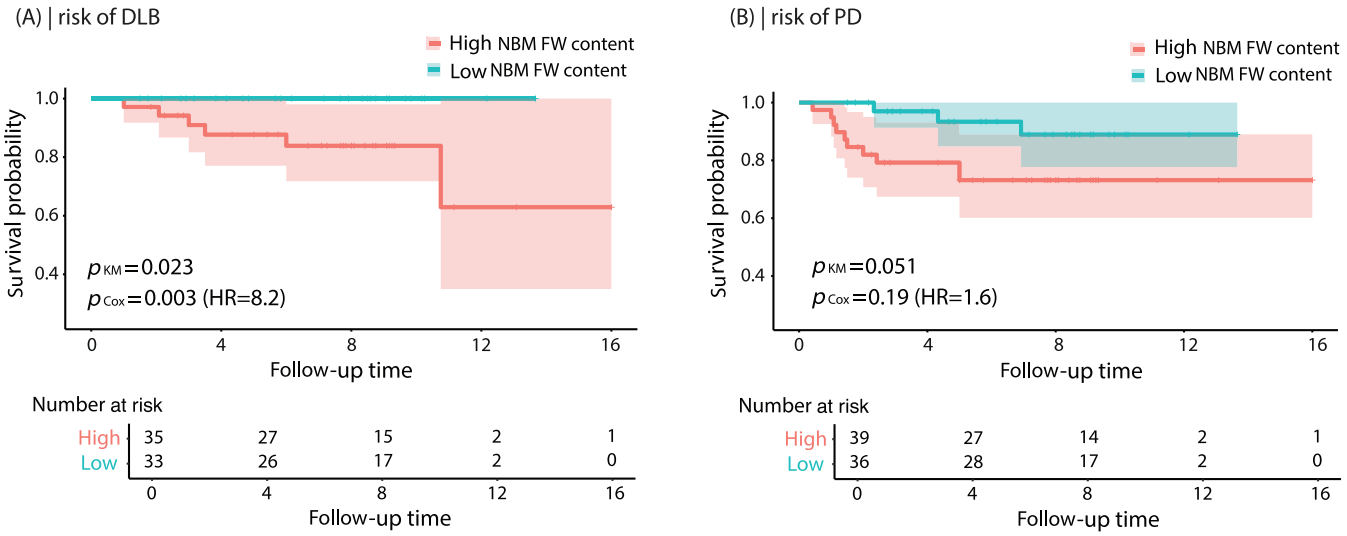

FIGURE 5 Kaplan–Meier survival curves showing association of FW content in NBM to predict phenoconversion risk to (A) DLB and (B) PD compared to remaining disease-free in iRBD. High FW content based on median FW level is represented in red, and low FW content is represented in blue. Shaded areas indicate 95% confidence intervals for each group. DLB, dementia with Lewy bodies; FW, free water; HR, hazard ratio; iRBD, isolated REM sleep behavior disorder; KM, Kaplan-Meier; NBM, nucleus basalis of Meynert; PD, Parkinson's disease; pSN, posterior substantia nigra.

earliest stages of disease, with studies reporting increases within the first year of diagnosis in *de novo* PD patients.[20,56] In iRBD, a prodromal synucleinopathy where over 90% of patients progress to either DLB (43.5%) or PD (56.5%),[1,2,57] FW imaging has yielded mixed findings. Although two studies reported increased FW in the posterior SN and NBM,[28,31] another found no significant FW differences in the posterior SN between iRBD patients and controls.[36] In our study, we similarly found no group-level FW differences in the NBM or posterior SN when comparing all iRBD patients to controls. However, when stratifying iRBD patients based on their phenoconversion status, FW content in both the NBM and posterior SN significantly differed between groups. This indicates that FW changes are not associated with the mere presence of iRBD but rather with its progression, supporting the notion that FW is better suited as a prognostic marker than a diagnostic one. These FW differences parallel previous neuroimaging findings in iRBD, including basal forebrain atrophy,[58–60] reduced neuromelanin signal in the SN,[61] and decreased nigrostriatal dopaminergic function.[62]

Importantly, we observed that FW increases in the NBM were specifically associated with disease progression toward DLB. Higher FW content in the NBM consistently predicted conversion to DLB, rather than PD or stable disease, even after adjusting for age and sex. Even when considering FW in the posterior SN as a covariate, ORs indicated that each SD increase in FW was associated with a seven-fold higher risk of developing DLB compared to remaining disease-free in iRBD and a four-fold higher risk of developing DLB compared to developing PD, underscoring the strong predictive utility of NBM FW for DLB conversion. These findings align with recent multimodal brain-clinical models, such as a multivariate SPECT perfusion signature implicating the basal forebrain in predicting DLB versus PD trajectories in iRBD.[10] Similarly, basal forebrain atrophy in iRBD has been reported[9,63] and linked to cognitive impairment,[58] and reduced cortical acetylcholinesterase activity has been associated with microglial activation in the SN.[64] Longitudinal data further suggest that cholinergic dysfunction in iRBD worsens over time,[65] reinforcing the vulnerability of the cholinergic system in prodromal DLB. Our results are also in line with studies showing increased FW in the NBM of patients with DLB.[35] In addition, NBM atrophy has been observed in iRBD patients with mild cognitive impairment,[60] a condition considered a strong risk factor for DLB phenoconversion.[66] Importantly, in this study, we demonstrate that despite showing NBM atrophy, only FW in the NBM is retained as a significant predictor of the development of DLB in iRBD. This extends the literature by showing that structural changes in the NBM, as indexed by FW, can serve as an early and specific marker of conversion to DLB in iRBD. That FW content in the posterior SN did not distinguish between DLB and PD converters may reflect the overlap in parkinsonian motor features shared by both disorders, which are less useful for predicting differential clinical trajectories.[46]

This study had some limitations. First, although it represents the largest currently available cohort of brain MRI scans from vPSG-confirmed iRBD patients and demonstrates the feasibility of using FW as a biomarker across sites with heterogeneous imaging protocols, the number of patients who had phenoconverted to PD or DLB remains limited. Larger samples of converters and replication in independent cohorts will be essential to strengthen the generalizability of our findings. Second, we focused on phenoconversion to DLB and PD due to the small number of patients who developed MSA (n = 4) or other conditions (n = 6). Future studies should aim to include a more representative sample of MSA cases to better characterize the full spectrum of phenoconversion trajectories. Third, only a single MRI time point was available for each participant, which precludes the longitudinal assessment of FW dynamics over time. Fourth, clinical phenotyping

across sites was limited to common variables (MoCA and MDS-UPDRS-III), and future multicentric efforts should harmonize more comprehensive clinical and neuropsychological assessments to better understand the clinical correlates of early FW changes. Fifth, *APOE* ε4 carrier status, despite its known association with faster progression to DLB,[67] was not available in this dataset and could not be considered in the analyses. Sixth, region-specific challenges in quality control, particularly in the NBM due to its proximity to CSF-filled spaces, led to a reduced sample size for this region. This highlights the need for robust and automated segmentation tools tailored to deep basal forebrain structures. Nevertheless, analyses of FW in the NBM and posterior SN conducted in the same subset of participants yielded findings consistent with those from the full sample, mitigating concerns about selection bias. Finally, this study did not assess how FW changes related to other early neurodegeneration biomarkers (e.g., positron emission tomography, neuromelanin MRI, or CSF markers), which may provide additional insight into underlying pathophysiological processes.

In summary, this large, multicenter, prospective study highlights the potential of FW imaging, particularly in the NBM, as a non-invasive biomarker for identifying iRBD patients at increased risk of phenoconversion to DLB. These findings support the integration of FW measures into future prognostic frameworks for prodromal synucleinopathies.

AUTHOR CONTRIBUTIONS

Celine Haddad contributed to data analysis and draft writing. Véronique Daneault contributed to data analysis and draft writing. Violette Ayral contributed to draft analysis and manuscript revision. Marie Filiatrault contributed to draft analysis and manuscript revision. Alexandre Pastor-Bernier contributed to draft analysis and manuscript revision. Christina Tremblay contributed to draft analysis and manuscript revision. Arnaud Boré contributed to draft analysis and manuscript revision. Maxime Descoteaux contributed to draft analysis and manuscript revision. Andrew Vo contributed to draft analysis and manuscript revision. Jean-François Gagnon contributed to data collection and manuscript revision. Ronald B. Postuma contributed to data collection and manuscript revision. Petr Dusek contributed to data collection and manuscript revision. Stanislav Marecek contributed to data collection and manuscript revision. Zsoka Varga contributed to data collection and manuscript revision. Johannes Klein contributed to data collection and manuscript revision. Michele T. Hu contributed to data collection and manuscript revision. Stéphane Lehéricy contributed to data collection and manuscript revision. Isabelle Arnulf contributed to data collection and manuscript revision. Marie Vidailhet contributed to data collection and manuscript revision. Jean-Christophe Corvol contributed to data collection and manuscript revision. Shady Rahayel contributed to data analysis, draft writing and study supervision.

ACKNOWLEDGMENTS

This work was supported by funding grants awarded to S.R. from Parkinson Canada (PPG-2023-0000000122) and Alzheimer Society Canada (0000000082), and supported by a memorial donation honoring Gaetan Boulianne and Pierre-Claude Durivage to the Foundation of Hopital du Sacre-Coeur de Montreal in support of Parkinson's disease research at the Centre for Advanced Research in Sleep Medicine. S.R. also holds a research scholar award from the Fonds de recherche du Quebec-Sante and grants from The Michael J. Fox Foundation. C.H. holds scholarships from the Canadian Institutes of Health Research, the Quebec Bio-Imaging Network, and Parkinson's Foundation. The work performed by the investigators from the Montreal iRBD cohort was supported by the Canadian Institutes of Health Research, the Fonds de recherche du Quebec-Sante, and the W. Garfield Weston Foundation. Specifically, J.F.G. reports grants from the Fonds de recherche du Quebec-Sante, the Canadian Institutes of Health Research, the W. Garfield Weston Foundation, the National Institutes of Health/National Institute on Aging, and holds a Canada Research Chair in Cognitive Decline in Pathological Aging. R.B.P. reports grants and personal fees from the Fonds de recherche du Quebec-Sante, Canadian Institute of Health Research, Parkinson Canada, the W. Garfield Weston Foundation, the Michael J. Fox Foundation, the R. Howard Webster Foundation, Roche, and the National Institutes of Health, as well as personal fees from Takeda, Biogen, AbbVie, Curasen, Lilly, Novartis, Eisai, Paladin, Merck, Korro, Vaxxinity, Bristol Myers Squibb, and the International Parkinson and Movement Disorders Society, all outside the submitted work. The work performed by the investigators from the Prague iRBD cohort was supported by the Czech Health Research Council grant NU21-04-00535 and by project LX22NPO5107 (MEYS) financed by the European Union-Next Generation UE. The work performed by the investigators from the Oxford iRBD cohort was supported by Parkinson's UK (J-2101) and the National Institute of Health Research (NIHR) Oxford Biomedical Research Centre (BRC). The work performed by the investigators from Paris iRBD cohort was supported by grants from the Programme d'investissements d'avenir (ANR-10-IAIHU-06), the Paris Institute of Neurosciences–IHU (IAIHU-06), the Agence Nationale de la Recherche (ANR-11-INBS-0006), Électricité de France (Fondation d'Entreprise EDF), Biogen Inc., the Fondation Thérèse et René Planiol, the Fonds Saint-Michel; by unrestricted support for research on PD from Energipole (M. Mallart) and Société Française de Médecine Esthétique (M. Legrand); and by a grant from the Institut de France to Isabelle Arnulf (for the Alice Study). The Parkinson's Progression Markers Initiative (PPMI) – a public-private partnership – is funded by the Michael J. Fox Foundation for Parkinson's Research and funding partners, including 4D Pharma, AbbVie Inc., AcureX Therapeutics, Allergan, Amathus Therapeutics, Aligning Science Across Parkinson's (ASAP), Avid Radiopharmaceuticals, Bial Biotech, Biogen, BioLegend, Bristol Myers Squibb, Calico Life Sciences LLC, Celgene Corporation, DaCapo Brainscience, Denali Therapeutics, The Edmond J. Safra Foundation, Eli Lilly and Company, GE Healthcare, GlaxoSmithKline, Golub Capital, Handl Therapeutics, Insitro, Janssen Pharmaceuticals, Lundbeck, Merck & Co., Inc., Meso Scale Diagnostics, LLC, Neurocrine Biosciences, Pfizer Inc., Piramal Imaging, Prevail Therapeutics, F. Hoffman-La Roche Ltd. and its affiliated company Genentech Inc., Sanofi Genzyme, Servier, Takeda Pharmaceutical Company, Teva Neuroscience, Inc., UCB, Vanqua Bio, Verily Life Sciences, Voyager Therapeutics, Inc., and Yumanity Therapeutics, Inc. For up-to-date information on the study, visit www.ppmi-info.org. Role of

the funding source: The funders had no role in data collection, analysis, interpretation, or writing of the manuscript. The corresponding author had full access to all study data and the final decision to submit for publication.

CONFLICT OF INTEREST STATEMENT

The authors declare no conflicts of interest. Author disclosures are available in the Supporting Information.

CONSENT STATEMENT

All study participants provided written, informed consent.

ORCID

Celine Haddad https://orcid.org/0009-0008-7737-2917

REFERENCES

1. Hogl B, Stefani A, Videnovic A. Idiopathic REM sleep behaviour disorder and neurodegeneration—an update. *Nat Rev Neurol*. 2018;14(1):40-55.
2. Galbiati A, Verga L, Giora E, Zucconi M, Ferini-Strambi L. The risk of neurodegeneration in REM sleep behavior disorder: a systematic review and meta-analysis of longitudinal studies. *Sleep Med Rev*. 2019;43:37-46.
3. Rahayel S, Tremblay C, Vo A, et al. Brain atrophy in prodromal synucleinopathy is shaped by structural connectivity and gene expression. *Brain*. 2022;145(9):3162-3178.
4. Rahayel S, Tremblay C, Vo A, et al. Mitochondrial function-associated genes underlie cortical atrophy in prodromal synucleinopathies. *Brain*. 2023;146(8):3301-3318.
5. Rahayel S, Postuma RB, Montplaisir J, et al. A prodromal brain-clinical pattern of cognition in synucleinopathies. *Ann Neurol*. 2021;89(2):341-357.
6. Rahayel S, Postuma RB, Montplaisir J, et al. Cortical and subcortical gray matter bases of cognitive deficits in REM sleep behavior disorder. *Neurology*. 2018;90(20):e1759-e1770.
7. Shin JH, Kim H, Kim YK, et al. Longitudinal evolution of cortical thickness signature reflecting Lewy body dementia in isolated REM sleep behavior disorder: a prospective cohort study. *Transl Neurodegener*. 2023;12(1):27.
8. Campabadal A, Segura B, Junque C, Iranzo A. Structural and functional magnetic resonance imaging in isolated REM sleep behavior disorder: a systematic review of studies using neuroimaging software. *Sleep Med Rev*. 2021;59:101495.
9. Eisenstein T, Groenewald K, van Hillegondsberg L, et al. Cholinergic degeneration in prodromal and early Parkinson's: a link to present and future disease states. *Brain*. 2025.
10. Rahayel S, Postuma R, Baril AA, et al. (99m)Tc-HMPAO SPECT perfusion signatures associated with clinical progression in patients with isolated rem sleep behavior disorder. *Neurology*. 2024;102(4):e208015.
11. Carli G, Meles SK, Reesink FE, et al. Comparison of univariate and multivariate analyses for brain [18F]FDG PET data in alpha-synucleinopathies. *Neuroimage Clin*. 2023;39:103475.
12. Carli G, Meles SK, Janzen A, et al. Occipital hypometabolism is a risk factor for conversion to Parkinson's disease in isolated REM sleep behaviour disorder. *Eur J Nucl Med Mol Imaging*. 2023;50(11):3290-3301.
13. Kim R, Lee JY, Kim YK, et al. Longitudinal changes in isolated rapid eye movement sleep behavior disorder-related metabolic pattern expression. *Mov Disord*. 2021;36(8):1889-1898.
14. Orso B, Mattioli P, Yoon EJ, et al. Validation of the REM behaviour disorder phenoconversion-related pattern in an independent cohort. *Neurol Sci*. 2023;44(9):3161-3168.
15. Arnaldi D, Mattioli P, Raffa S, et al. Presynaptic dopaminergic imaging characterizes patients with REM sleep behavior disorder due to synucleinopathy. *Ann Neurol*. 2024;95(6):1178-1192.
16. Iranzo A, Stefani A, Ninerola-Baizan A, et al. Left-hemispheric predominance of nigrostriatal deficit in isolated REM sleep behavior disorder. *Neurology*. 2020;94(15):e1605-e1613.
17. Chahine LM, Brumm MC, Caspell-Garcia C, et al. Dopamine transporter imaging predicts clinically-defined alpha-synucleinopathy in REM sleep behavior disorder. *Ann Clin Transl Neurol*. 2021;8(1):201-212.
18. Miglis MG, Adler CH, Antelmi E, et al. Biomarkers of conversion to alpha-synucleinopathy in isolated rapid-eye-movement sleep behaviour disorder. *Lancet Neurol*. 2021;20(8):671-684.
19. Pasternak O, Sochen N, Gur Y, Intrator N, Assaf Y. Free water elimination and mapping from diffusion MRI. *Magn Reson Med*. 2009;62(3):717-730.
20. Burciu RG, Ofori E, Archer DB, et al. Progression marker of Parkinson's disease: a 4-year multi-site imaging study. *Brain*. 2017;140(8):2183-2192.
21. Ofori E, Pasternak O, Planetta PJ, et al. Increased free water in the substantia nigra of Parkinson's disease: a single-site and multi-site study. *Neurobiol Aging*. 2015;36(2):1097-1104.
22. Ofori E, Pasternak O, Planetta PJ, et al. Longitudinal changes in free-water within the substantia nigra of Parkinson's disease. *Brain*. 2015;138:2322-2331.
23. Chen M, Wang Y, Zhang C, et al. Free water and iron content in the substantia nigra at different stages of Parkinson's disease. *Eur J Radiol*. 2023;167:111030.
24. Arribarat G, Pasternak O, De Barros A, Galitzky M, Rascol O, Peran P. Substantia nigra locations of iron-content, free-water and mean diffusivity abnormalities in moderate stage Parkinson's disease. *Parkinsonism Relat Disord*. 2019;65:146-152.
25. Zhou G, Ren J, Rong D, et al. Monitoring substantia nigra degeneration using free water imaging across prodromal and clinical Parkinson's disease. *Mov Disord*. 2023;38(5):774-782.
26. Guttuso T, Jr, Bergsland N, Hagemeier J, Lichter DG, Pasternak O, Zivadinov R. Substantia nigra free water increases longitudinally in Parkinson's Disease. *AJNR Am J Neuroradiol*. 2018;39(3):479-484.
27. Bae YJ, Kim JM, Sohn CH, et al. Imaging the substantia nigra in Parkinson disease and other parkinsonian syndromes. *Radiology*. 2021;300(2):260-278.
28. Zhou L, Li G, Zhang Y, et al. Increased free water in the substantia nigra in idiopathic REM sleep behaviour disorder. *Brain*. 2021;144(5):1488-1497.
29. Ofori E, Krismer F, Burciu RG, et al. Free water improves detection of changes in the substantia nigra in parkinsonism: a multisite study. *Mov Disord*. 2017;32(10):1457-1464.
30. Ray NJ, Lawson RA, Martin SL, et al. Free-water imaging of the cholinergic basal forebrain and pedunculopontine nucleus in Parkinson's disease. *Brain*. 2023;146(3):1053-1064.
31. Zhang D, Zhou L, Lu C, Feng T, Liu J, Wu T. Free-Water imaging of the nucleus basalis of meynert in patients with idiopathic REM sleep behavior disorder and Parkinson's Disease. *Neurology*. 2024;102(7):e209220.
32. Wang C, Wang S, Zhou C, et al. LRRK2 mutation contributes to decreased free water in the nucleus basalis of Meynert in manifest and premanifest Parkinson's disease. *J Neurol*. 2024;272(1):33.
33. Crowley SJ, Amin M, Tanner JJ, Ding M, Mareci TA, Price CC. Free water fraction predicts cognitive decline for individuals with idiopathic Parkinson's disease. *Parkinsonism Relat Disord*. 2022;104:72-77.

34. Crowley SJ, Kanel P, Roytman S, Bohnen NI, Hampstead BM. Basal forebrain integrity, cholinergic innervation and cognition in idiopathic Parkinson's disease. *Brain*. 2024;147(5):1799-1808.
35. Schumacher J, Ray NJ, Hamilton CA, et al. Free water imaging of the cholinergic system in dementia with Lewy bodies and Alzheimer's disease. *Alzheimers Dement*. 2023;19(10):4549-4563.
36. Tobin ER, Arpin DJ, Schauder MB, et al. Functional and free-water imaging in rapid eye movement behaviour disorder and Parkinson's disease. *Brain Commun*. 2024;6(5):fcae344.
37. Gan-Or Z, Rao T, Leveille E, et al. The quebec parkinson network: a researcher-patient matching platform and multimodal biorepository. *J Parkinsons Dis*. 2020;10(1):301-313.
38. Marek K, Chowdhury S, Siderowf A, et al. The Parkinson's progression markers initiative (PPMI)—establishing a PD biomarker cohort. *Ann Clin Transl Neurol*. 2018;5(12):1460-1477.
39. Medicine AAoS. *The* International Classification of Sleep Disorders — Third Edition (ICSD-3). 3rd ed. American Academy of Sleep Medicine; 2014.
40. McKeith IG, Boeve BF, Dickson DW, et al. Diagnosis and management of dementia with Lewy bodies: fourth consensus report of the DLB Consortium. *Neurology*. 2017;89(1):88-100.
41. Postuma RB, Berg D, Stern M, et al. MDS clinical diagnostic criteria for Parkinson's disease. *Mov Disord*. 2015;30(12):1591-1601.
42. Wenning GK, Stankovic I, Vignatelli L, et al. The movement disorder society criteria for the diagnosis of multiple system atrophy. *Mov Disord*. 2022;37(6):1131-1148.
43. Nasreddine ZS, Phillips NA, Bedirian V, et al. The Montreal Cognitive Assessment, MoCA: a brief screening tool for mild cognitive impairment. *J Am Geriatr Soc*. 2005;53(4):695-699.
44. Goetz CG, Tilley BC, Shaftman SR, et al. Movement disorder society-sponsored revision of the unified Parkinson's disease rating scale (MDS-UPDRS): scale presentation and clinimetric testing results. *Mov Disord*. 2008;23(15):2129-2170.
45. Ayral V, Pastor-Bernier A, Daneault V, et al. Glymphatic defect in isolated REM sleep behavior disorder is associated with phenoconversion to Parkinson's disease. *Neurology*. Forthcoming 2025.
46. Joza S, Delva A, Tremblay C, et al. Distinct brain atrophy progression subtypes underlie phenoconversion in isolated REM sleep behaviour disorder. *EBioMedicine*. 2025;117:105753.
47. Theaud G, Houde JC, Bore A, Rheault F, Morency F, Descoteaux M. TractoFlow: a robust, efficient and reproducible diffusion MRI pipeline leveraging Nextflow & Singularity. *Neuroimage*. 2020;218:116889.
48. Kurtzer GM, Sochat V, Bauer MW. Singularity: scientific containers for mobility of compute. *PLoS One*. 2017;12(5):e0177459.
49. Di Tommaso P, Chatzou M, Floden EW, Barja PP, Palumbo E, Notredame C. Nextflow enables reproducible computational workflows. *Nat Biotechnol*. 2017;35(4):316-319.
50. Daducci A, Canales-Rodriguez EJ, Zhang H, Dyrby TB, Alexander DC, Thiran JP. Accelerated microstructure imaging via convex optimization (AMICO) from diffusion MRI data. *Neuroimage*. 2015;105:32-44.
51. Gaser C, Dahnke R, Thompson PM, Kurth F, Luders E, The Alzheimer's Disease Neuroimaging I. CAT: a computational anatomy toolbox for the analysis of structural MRI data. *Gigascience*. 2024;13:giae049.
52. Fortin JP, Cullen N, Sheline YI, et al. Harmonization of cortical thickness measurements across scanners and sites. *Neuroimage*. 2018;167:104-120.
53. Orlhac F, Eertink JJ, Cottereau AS, et al. A Guide to ComBat harmonization of imaging biomarkers in multicenter studies. *J Nucl Med*. 2022;63(2):172-179.
54. Fortin JP, Parker D, Tunc B, et al. Harmonization of multi-site diffusion tensor imaging data. *Neuroimage*. 2017;161:149-170.
55. Andica C, Kamagata K, Hatano T, et al. Free-Water imaging in white and gray matter in Parkinson's. *Disease Cells*. 2019;8(8).
56. Schulz J, Pagano G, Fernandez Bonfante JA, Wilson H, Politis M. Nucleus basalis of Meynert degeneration precedes and predicts cognitive impairment in Parkinson's disease. *Brain*. 2018;141(5):1501-1516.
57. Postuma RB, Iranzo A, Hu M, et al. Risk and predictors of dementia and parkinsonism in idiopathic REM sleep behaviour disorder: a multicentre study. *Brain*. 2019;142(3):744-759.
58. Yang A, Li G. Nucleus basalis of Meynert predicts cognitive changes in isolated REM sleep behavior disorder. *Sleep Med*. 2023;109:11-17.
59. Tan C, Nawaz H, Lageman SK, et al. Cholinergic nucleus 4 degeneration and cognitive impairment in isolated rapid eye movement sleep behavior disorder. *Mov Disord*. 2023;38(3):474-479.
60. Remillard-Pelchat D, Rahayel S, Gaubert M, et al. Comprehensive analysis of brain volume in rem sleep behavior disorder with mild cognitive impairment. *J Parkinsons Dis*. 2022;12(1):229-241.
61. Gaurav R, Pyatigorskaya N, Biondetti E, et al. Deep learning-based neuromelanin mri changes of isolated rem sleep behavior disorder. *Mov Disord*. 2022;37(5):1064-1069.
62. Arnaldi D, Chincarini A, Hu MT, et al. Dopaminergic imaging and clinical predictors for phenoconversion of REM sleep behaviour disorder. *Brain*. 2021;144(1):278-287.
63. Woo KA, Kim H, Kim R, et al. Cholinergic degeneration and early cognitive signs in prodromal Lewy body dementia. *Alzheimers Dement*. 2025;21(2):e14584.
64. Staer K, Iranzo A, Stokholm MG, et al. Cortical cholinergic dysfunction correlates with microglial activation in the substantia innominata in REM sleep behavior disorder. *Parkinsonism Relat Disord*. 2020;81:89-93.
65. Staer K, Iranzo A, Terkelsen MH, et al. Progression of brain cholinergic dysfunction in patients with isolated rapid eye movement sleep behavior disorder. *Eur J Neurol*. 2024;31(1):e16101.
66. Genier Marchand D, Montplaisir J, Postuma RB, Rahayel S, Gagnon JF. Detecting the cognitive prodrome of dementia with lewy bodies: a prospective study of REM sleep behavior disorder. *Sleep*. 2017;40(1):101093/sleep/zsw014.
67. Dickson DW, Heckman MG, Murray ME, et al. APOE epsilon4 is associated with severity of Lewy body pathology independent of Alzheimer pathology. *Neurology*. 2018;91(12):e1182-e95.

SUPPORTING INFORMATION

Additional supporting information can be found online in the Supporting Information section at the end of this article.

How to cite this article: Haddad C, Daneault V, Ayral V, et al. Free water predicts dementia with Lewy bodies in isolated REM sleep behavior disorder. *Alzheimer's Dement*. 2025;21:e70570. https://doi.org/10.1002/alz.70570

APPENDIX

List of contributors involved in the ICEBERG Study Group:

Steering committee: Marie Vidailhet, MD, PhD (Pitié-Salpêtrière Hospital, Paris, principal investigator of ICEBERG); Jean-Christophe Corvol, MD, PhD (Pitié-Salpêtrière Hospital, Paris, scientific lead); Isabelle Arnulf, MD, PhD (Pitié-Salpêtrière Hospital, Paris, member of steering committee); Stéphane Lehericy, MD, PhD (Pitié-Salpêtrière Hospital, Paris, member of steering committee).

Clinical data: Marie Vidailhet, MD, PhD (Pitié-Salpêtrière Hospital, Paris, coordination); Graziella Mangone, MD, PhD (Pitié-Salpêtrière Hospital, Paris, co-ordination); Jean-Christophe Corvol, MD, PhD (Pitié-Salpêtrière Hospital, Paris); Isabelle Arnulf, MD, PhD (Pitié-Salpêtrière Hospital, Paris); Sara Sambin, MD (Pitié-Salpêtrière Hospital, Paris); Jonas Ihle, MD (Pitié-Salpêtrière Hospital, Paris); Caroline Weill, MD (Pitié-Salpêtrière Hospital, Paris); David Grabli, MD, PhD (Pitié-Salpêtrière Hospital, Paris); Florence Cormier-Dequaire, MD (Pitié-Salpêtrière Hospital, Paris); Louise Laure Mariani, MD, PhD (Pitié-Salpêtrière Hospital, Paris); Bertrand Degos, MD, PhD (Avicenne Hospital, Bobigny).

Neuropsychological data: Richard Levy, MD (Pitié-Salpêtrière Hospital, Paris, coordination); Fanny Pineau, MS (Pitié-Salpêtrière Hospital, Paris, neuropsychologist); Julie Socha, MS (Pitié-Salpêtrière Hospital, Paris, neuropsychologist); Eve Benchetrit, MS (La Timone Hospital, Marseille, neuropsychologist); Virginie Czernecki, MS (Pitié-Salpêtrière Hospital, Paris, neuropsychologist); Marie-Alexandrine, MS (Pitié-Salpêtrière Hospital, Paris, neuropsychologist).

Eye movement: Sophie Rivaud-Pechoux, PhD (ICM, Paris, coordination); Elodie Hainque, MD, PhD (Pitié-Salpêtrière Hospital, Paris).

Sleep assessment: Isabelle Arnulf, MD, PhD (Pitié-Salpêtrière Hospital, Paris, coordination); Smaranda Leu Semenescu, MD (Pitié-Salpêtrière Hospital, Paris); Pauline Dodet, MD (Pitié-Salpêtrière Hospital, Paris).

Genetic data: Jean-Christophe Corvol, MD, PhD (Pitié-Salpêtrière Hospital, Paris, coordination); Graziella Mangone, MD, PhD (Pitié-Salpêtrière Hospital, Paris, co-coordination); Samir Bekadar, MS (Pitié-Salpêtrière Hospital, Paris, biostatistician); Alexis Brice, MD (ICM, Pitié-Salpêtrière Hospital, Paris); Suzanne Lesage, PhD (INSERM, ICM, Paris, genetic analyses).

Metabolomics: Fanny Mochel, MD, PhD (Pitié-Salpêtrière Hospital, Paris, coordination); Farid Ichou, PhD (ICAN, Pitié-Salpêtrière Hospital, Paris); Vincent Perlbarg, PhD, Pierre and Marie Curie University); Benoit Colsch, PhD (CEA, Saclay); Arthur Tenenhaus, PhD (Supelec, Gif-sur-Yvette, data integration).

Brain MRI data: Stéphane Lehericy, MD, PhD (Pitié-Salpêtrière Hospital, Paris, coordination); Rahul Gaurav, MS, (Pitié-Salpêtrière Hospital, Paris, data analysis); Nadya Pyatigorskaya, MD, PhD, (Pitié-Salpêtrière Hospital, Paris, data analysis); Lydia Yahia-Cherif, PhD (ICM, Paris, Biostatistics); Romain Valabregue, PhD (ICM, Paris, data analysis); Cécile Galléa, PhD (ICM, Paris).

DaTscan imaging data: Marie-Odile Habert, MCU-PH (Pitié-Salpêtrière Hospital, Paris, coordination);

Voice recording: Dijana Petrovska, PhD (Telecom Sud Paris, Evry, coordination); Laetitia Jeancolas, MS (Telecom Sud Paris, Evry).

Study management: Vanessa Brochard (Pitié-Salpêtrière Hospital, Paris, coordination); Alizé Chalançon (Pitié-Salpêtrière Hospital, Paris, Project manager); Carole Dongmo-Kenfack (Pitié-Salpêtrière Hospital, Paris, clinical research assistant); Christelle Laganot (Pitié-Salpêtrière Hospital, Paris, clinical research assistant); Valentine Maheo (Pitié-Salpêtrière Hospital, Paris, clinical research assistant).